Journal of Electroanalytical Chemistry 850 (2019) 113363

Contents lists available at ScienceDirect

Journal of Electroanalytical Chemistry

journal homepage: www.elsevier.com/locate/jelechem

Examination and prevention of ring collection failure during gas-evolving reactions on a rotating ring-disk electrode

J.G. Vos, M.T.M. Koper *

Leiden Institute of Chemistry, Leiden University, PO Box 9502, 2300 RA Leiden, the Netherlands

ARTICLE INFO

Article history:
Received 11 April 2019
Received in revised form 28 July 2019
Accepted 6 August 2019
Available online 07 August 2019

Keywords:
Rotating ring-disk electrode
Gas bubbles
Collection efficiency
Chlorine evolution
Oxygen evolution
Hydrogen evolution

ABSTRACT

Use of a rotating ring-disk electrode during gas-evolving reactions has been shown liable to errors under higher current densities, since product collection on the ring is vulnerable to the formation of gas bubbles at the disk-ring interspace. In this study, we explored methods of reducing such bubble-related errors and improving the reliability of the collection factor under high-intensity gas evolution. We attempted the mounting of a thin wire close to the surface, to dislodge bubbles that formed specifically on the interface between the disk and the disk-ring spacer. This approach was tested for the detection of chlorine during parallel chlorine and oxygen evolution, and resulted in a notable alteration of the collection efficiency; its value became lower than theoretical expectations and also quite stable, even under higher current densities. We also coated the RRDE tip in a hydrophilic polymer, to reduce the tendency of bubble formation; this was tested for the collection of hydrogen and oxygen gas, and led to a mild increase in overall performance. The coating allowed for approximately 50% higher hydrogen evolution current density without ring failure, and for oxygen collection led to an overall improvement in behaviour.

1. Introduction

Several of the most promising processes for alternatives to fossil fuels in the world energy infrastructure, such as water electrolysis and CO_2 reduction, are electrochemical reactions. Fundamental studies of the corresponding half-reactions are crucial for a cost-effective practical implementation. Such fundamental studies are often done using a rotating ring-disk electrode (RRDE), as this tool greatly increases the amount of information that can be obtained from an experiment when compared to a stationary electrode [1]. Furthermore, the secondary ring electrode can be used for collection experiments, where the extent of a reaction can be quantified by selectively reacting the corresponding product. This method offers a rapid and flexible means to determine selectivity in systems where parallel reaction pathways can occur and multiple products form simultaneously.

In collection experiments, an important quantity is the collection efficiency N, which is the (molar) fraction of products formed on the disk that are collected on the ring. It is defined as

$$N = \left|\frac{n_D i_R}{n_R i_D}\right| \quad (1)$$

where i_D and i_R are the ring and disk current belonging to the reaction occurring on the disk and the reaction occurring on the ring, respectively, and n_D and n_R are the numbers of electrons in these reactions. Often, the disk and ring reaction are simply each other's reverse, meaning that n_D and n_R are the same. Importantly, N is a constant that should only depend on the ring-disk geometry [1].

In many important processes, such as the evolution of H_2 and O_2 in water electrolysis, Cl_2 in the chlor-alkali and chlorate process, and CO_2 in direct alcohol fuel cells [2], the relevant reactions are gas-evolving reactions. Although the RRDE was not principally designed for reactions involving gas formation [3], it has been used quite extensively and successfully for this purpose. There is however also a significant body of literature showing that RRDE experiments involving gas formation on the disk are hindered by unreliability, or may even lead to strong ring collection failure in the sense that Eq. (1) does not give a reliable and stable value for N [4–22]. Our own findings during extensive work on OER and the chlorine evolution reaction (CER) confirm this tendency. The problem can be traced to gas supersaturation near the electrode surface, leading to the formation of bubbles [23–25]. Especially when the solubility of the product gas is low and there is heterogeneous distribution of current across the surface, as is often the case, supersaturation can easily occur. We believe this problem, in part, underlies the relative scarcity of studies attempting to use the RRDE to measure the faradaic efficiency of the OER or hydrogen evolution reaction (HER), despite the commercial availability of RRDE systems and their widespread use in the study of the closely-related oxygen reduction reaction, which does not involve gas evolution [26–28].

* Corresponding author.
E-mail address: m.koper@chem.leidenuniv.nl (M.T.M. Koper).

https://doi.org/10.1016/j.jelechem.2019.113363

During gas evolution, both nano and macro sized bubbles may form. Nanoscale bubbles nucleate directly on the electroactive surface, and can transiently isolate active surface sites or block transport through pores in case of a porous electrode, leading to irregularities in the current-potential response. This problem has been well-described in previous publications [29–32]. Here, we focus exclusively on adhering macroscopic bubbles, which are large enough to be seen with the naked eye, and their disrupting effect on the hydrodynamic flow between disk and ring on an RRDE. From previous reports and our own experience, such bubbles adhere strongly to the spacer between the disk and the ring, especially when the spacer is made out of highly hydrophobic materials, such as PTFE [23]. This accumulation of bubbles at the spacer affects strongly the collection factor *N* by forming a physical barrier that can decrease *N* in an erratic way. Furthermore, the gas in the bubbles, which is part of the product that originates from disk, is not properly detected by the ring, making accurate quantification impossible. In previous experiments involving the collection of H_2, *N* was prone to erratic behaviour and strongly decreased when the HER current density exceeded a certain threshold; it also typically had a value persistently lower than the theoretical *N* before reaching that threshold [4,15,17,16]. Similar results were reported concerning O_2 collection during OER [6–12,18–22,13]. Many authors have resorted to an empirical correction, based on measurements of *N* in comparable experiments where its value should be ideal [5,8,9,11,12,14,19,22,13].

Several solutions to lessen bubble adhesion have been suggested; Kadija et al. proposed the use of a rotating ring electrode (RRE) [3], optionally equipped with a secondary ring, leading to the rotating ring-ring electrode (RRRE) [23,33,34]. The RRRE offers the advantage of increased liquid momentum at the electroactive areas to aid bubble detachment, which can be tuned using the ring diameter. A rotating ring cone electrode (RRCE) was also suggested, which has a vertically angled electroactive surface, and uses gas bubble buoyancy to promote detachment [35–37]. In another case, a liquid jet was used to intermittently remove accumulated gas bubbles from the electrode surface [38]. Despite the obvious advantages of the RRRE and RRCE and the significant research efforts that have gone into their development, today the RRDE is still the most widely used rotating electrode geometry, even for gas-evolving reactions. It is more easily fabricated and prepared for analytic electrochemical studies, which often require very high purity conditions and the possibility for fast throughput.

As described above, we have made extensive use of the RRDE for quantification of gaseous products, but constant vigilance was needed during the experiments to ensure reproducible ring-disk collection properties. In this paper we describe our attempts to improve the gas collection behaviour of a typical RRDE setup. As test system, we studied the evolution of Cl_2, O_2 and H_2, gases that have great electrocatalytic significance, as described above. We will report results from two approaches: i) one involving the careful placement of a thin Ti wire very close to the interface of the disk and the Teflon spacer, to physically dislodge bubbles stuck at this interface, and ii) coating the RRDE tip assembly with the hydrophilic polymer poly-dopamine (p-DA), in an attempt to decrease the tendency of hydrophobic bubble formation on the surface.

2. Experimental

2.1. Chemicals

$HClO_4$ (70%, Suprapur/Trace analysis grade), KCl (EMSURE/Analysis grade), KOH solution (32%, EMSURE/Analysis grade), HCl (30%, Ultrapur/Trace analysis grade) and $KHSO_4$ (EMSURE/Analysis grade) were purchased from Merck. All purchased chemicals were used as received. The water used for all experiments was prepared by a Merck Millipore Milli-Q system (resistivity 18.2 MΩcm, TOC < 5 p.p.b.).

2.2. Cleaning procedures

All experiments were carried out at room temperature (~20 °C).

Electrochemical experiments except those involving a Ti wire near the tip were done using home-made two-compartment borosilicate glass cells with solution volumes of 100 mL. Experiments with the Ti wire were done in a single compartment vial of approximately 16 mL volume. Before first-time use, all glassware was thoroughly cleaned by boiling in a 3:1 mixture of concentrated H_2SO_4 and HNO_3. When not in use, all glassware was stored in a 0.5 M H_2SO_4 solution containing 1 g/L $KMnO_4$. Before each experiment, glassware was thoroughly rinsed with water, and then submerged in a dilute (~0.01 M) solution of H_2SO_4 and H_2O_2 to remove all traces of $KMnO_4$ and MnO_2. The glassware was then rinsed three times with water and boiled in water. The rinsing-boiling procedure was repeated two more times.

2.3. Cell preparation

All experiments were done with a MSR rotator and E6 ChangeDisk RRDE tips in a PEEK shroud (Pine Research). An IviumStat potentiostat (Ivium Technologies) was used for potential control during electrochemistry experiments. All experiments were 95% iR-compensated in-situ. The solution resistance was measured with electrochemical impedance spectroscopy at 1.30 V vs. RHE (IrO_x/GC disk working electrode) or 0.05 V vs. RHE (Pt disk working electrode), by observing the absolute impedance in the high frequency domain (100–50 KHz) corresponding to a zero-degree phase angle. All used solutions were saturated with Ar (Linde, purity 6.0) before experiments. During forced convection experiments, solutions were continuously bubbled with Ar gas, in stationary conditions, Ar was used to blanket the solution. In experiments involving the placing of a Ti wire close to the RRDE tip, the reference electrode was a LowProfile Ag/AgCl electrode (Pine Research, E = 198 mV vs. NHE). In all other experiments, the reference electrode was a HydroFlex® reversible hydrogen electrode (Gaskatel), separated from the main solution using a Luggin capillary. All potentials in this paper are reported on the RHE scale. A Pt mesh was used as counter electrode, separated from the main solution with a coarse sintered glass frit.

2.4. Electrode preparation

GC disks (Pine Research Instrumentation, surface area 0.196 cm^2) were prepared to a mirror finish by hand polishing on Microcloth pads with diamond paste suspensions down to 0.05 μm particle size (Buehler), followed by rinsing and sonication of the electrode in water for 3 min. A thin layer of hydrous IrO_x was then deposited onto the GC via electroflocculation of IrO_x nanoparticles from a meta-stable IrO_x colloid suspension [39–42]. In experiments involving a Pt disk working electrode, the assembled tip was treated for 3 min with a solution of 0.5 M H_2SO_4 containing 0.5 g/L $KMnO_4$, followed by rinsing with water, treatment with a dilute (~0.01 M) solution of H_2SO_4 and H_2O_2 to remove any traces of $KMnO_4$ and MnO_2, and further extensive rinsing with water. During RRDE experiments, any Pt electrode (the Pt ring or, if used, the Pt disk) was electropolished by scanning from −0.1 V to 1.7 V at 500 mV s^{-1} for 20 scans at 1500 RPM. In-between experiments, the disk electrode was kept either at 1.3 V vs. RHE (IrO_x/GC working electrode) or 0.05 V (Pt working electrode). Ring currents were corrected for constant background currents and product collection delay. The latter arises from the time needed for products formed on the disk to reach the ring, and was approximately 200 ms at 1500 RPM. Poly-dopamine (p-DA) deposition was done by submerging the Pt-Pt RRDE in a 20 mM sodium phosphate solution of pH ≈ 7, containing 2 g/L dopamine (DA). The tip was kept in the solution for 1 h under gentle rotation (300 RPM), after which it was thoroughly rinsed with water.

3. Results and discussion

3.1. Examples of ring failure during gas collection experiments

We will first present some extreme examples of ring collection failure, measured during the study of parallel oxygen evolution and chlorine evolution, as well as only chlorine evolution. In this section and in Section 3.2, we will particularly discuss the collection of Cl_2, which often forms in combination with O_2. To prevent confusion, the various collection factors will be labelled according to the species that are measured. Disk and ring currents were both normalized versus the disk geometrical surface area (the ring surface area is irrelevant since it is always used as a detector, such that all ring reactions are diffusion limited).

In previous work, we have shown that operating a RRDE with a Pt ring at 0.95 V allows selective probing of Cl_2 evolved on the disk, provided that the solution is strongly acidic (pH < 1) [43]. Compared to O_2, the aqueous solubility of Cl_2 is rather high, even at this low pH [44], such that it was possible to use this method up until relatively large CER current densities without the formation of Cl_2 bubbles. However, the formation of poorly soluble O_2 in parallel with Cl_2 strongly increases the probability of bubble formation, and limits the maximum potential at which the method is still reliable. On highly OER-active GC-supported IrO_x, this limit was determined by roughly 10 mA cm^{-2}, usually reached close to 1.55 V vs. RHE. Fig. 1A illustrates the difficulties that arise when attempting measurements at higher potential.

In Fig. 1A, parallel OER and CER on the disk leads to a continuously increasing current with more positive potential. The ring current density, which selectively probes CER, is expected to rise initially, concomitantly with the disk current, and then to level off to a limiting value as the CER on the disk becomes fully mass-transfer controlled. Instead, we observe a sharp and consistent *decrease* in the ring current density as the potential increases above 1.56 V ($\eta_{CER} \approx 170$ mV), as well as increasing noise in the signal. As mentioned, it is likely that under these conditions, the formation of O_2 bubbles disrupts the transport of Cl_2 from the disk to the ring. In our experience, once gas bubbles of a poorly soluble species form, such as O_2, they do so irreversibly: they stick to the electrode tip persistently, regardless of ring or disk potential, or solution flow. This is illustrated in the backward scan in Fig. 1A, where the ring does not recover its collection efficiency, even at potentials for which the disk current has decreased to lower values than in the forward scan where the collection efficiency was still well-behaved. We also found that even under high rotation rates (>2500 RPM), the time for any formed bubbles to completely dissolve can be very long. During this period the ring collection factor is distorted and cannot be trusted. The transient nature of gas collection failure is further illustrated in Fig. 1B. In this experiment, evolution and collection of Cl_2 was performed on a Pt-Pt RRDE in a concentrated chloride solution (1 M HCl), with varying scan rates. CER currents on the disk measure (industrially relevant [45]) densities in the range of 1 kA m^{-2}. Initially the ring current density follows, but at the slowest scan rate of 10 mV s^{-1}, N_{Cl_2} starts decreasing at approximately 1.4 V vs. RHE ($\eta_{CER} \approx 145$ mV), corresponding to 100 mA cm^{-2}_{Disk}. At around 1.49 V ($\eta_{CER} \approx 235$ mV), the ring fails catastrophically; this is presumably due to extensive formation of Cl_2 bubbles. The 'potential of failure' shifts to higher values for higher scan rates, suggesting that it is strongly dependent on the local build-up of gas.

In general, we find that presence of gas bubbles may not be noticeable from the ring response at first glance, as long as the bubbles are small and not too numerous. In this case, the only clear indication of transport distortion on the tip is usually an unexpectedly but reproducibly low collection factor, and perhaps a subtle periodic noise in the signal that can be rotation rate dependent. Before and in-between repeated gas evolution experiments, we recommend thorough visual inspection of the electrode tip; it is strongly advised to do this while rotation is switched off. Once it has been verified that the working electrode tip is completely free of bubbles, one can check for gas bubble interference over the course of an experiment by scanning the relevant potential window repeatedly, or by changing the scan rate. If the collection factor is reproducible during this straight-forward control experiment, no gas bubbles should have formed. A practical solution for removing persistent bubbles was to lift the electrode tip just above the working solution within the cell, rotate it momentarily to spin away liquid and bubbles, and then re-immerse it.

3.2. RRDE voltammetry experiments using a blocking wire

During our experiments, we saw that gas bubbles usually appear on the disk-ring interspace, which in our case is made of Teflon. Bubbles were especially prone to adhere near the disk boundary (Fig. 2A). Once formed, they may grow by absorbing highly concentrated gas in the nearby solution, which aggravates the problem and may explain why the ring function is usually irrecoverable after failure.

Our initial, rather simple-minded attempt at preventing bubble interference was to prevent bubbles from accumulating, by specifically targeting the disk-Teflon boundary. To do so, we carefully installed an

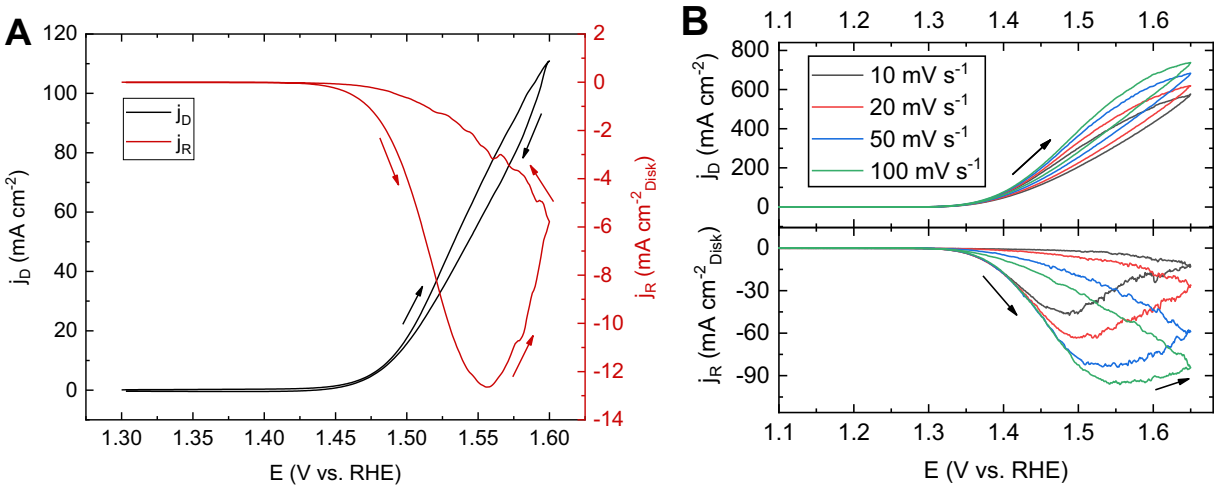

Fig. 1. Illustration of RRDE ring failure during gas evolution. Panel A: Parallel OER and CER on an IrO_x/GC disk, with the Pt ring fixed at 0.95 V vs. RHE to selectively probe Cl_2. Solution: 0.5 M $KHSO_4$ + 100 mM KCl saturated with Ar, rotation rate 1500 RPM. B: Evolution of (mainly) Cl_2 on a Pt disk, while again keeping the ring fixed at 0.95 V, with varying scan rate. Solution: 1 M HCl saturated with Ar, rotation rate 1500 RPM. Arrows indicate scan directions.

Fig. 2. Photographs of a rotating electrode equipped with an IrO_x/GC disk (black) and Pt ring (grey). A: Tip after an experiment involving vigorous gas evolution, during which the collection factor became severely distorted. B: Tip during attempts to dislodge gas bubbles using a Ti wire. The Ti wire is mounted under the tip, with its point aimed at the disk-Teflon spacer boundary. Accumulating bubbles collided with the wire and were 'pushed off' during rotation.

acid etched and flame-annealed Ti wire very close to the surface of the tip (Fig. 2B). The wire was made long and as thin as possible, to minimize effects that it might have on the fluid dynamics near the rotating tip.

Fig. 3A shows results of RDDE experiments with a Ti wire, and its effect on the ring current density and N_{Cl_2} during intense evolution of O_2 and Cl_2 gas. During large currents, we observed continuous formation of bubbles over the disk electrode surface during rotation. The Ti wire

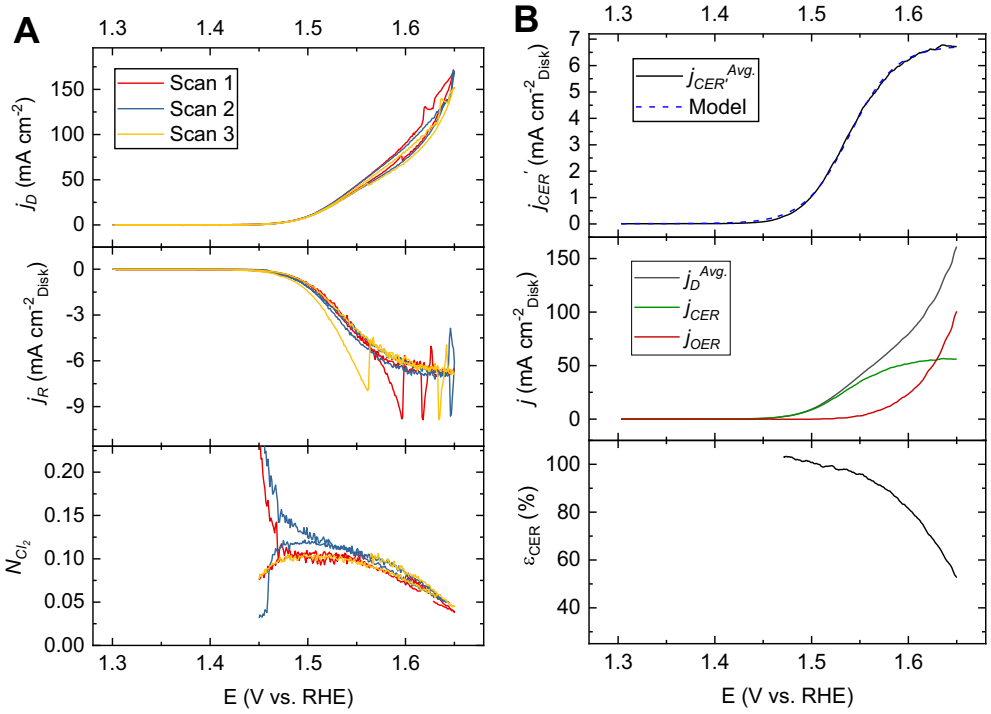

Fig. 3. RRDE gas evolution experiments with the point of a Ti wire mounted close to the disk-spacer boundary (see Fig. 2B). A: Repeated scans into the mixed OER + CER potential region, where vigorous gas evolution occurs. As in Fig. 1A, the active catalyst is IrO_x/GC, and a Pt ring at 0.95 V was used to selectively detect Cl_2. Shown are disk (top panel) and ring current density (middle panel), as well as the collection efficiency N_{Cl_2} (bottom panel). Scan rate: 10 mV s^{-1}. Solution: 0.5 M $KHSO_4$ + 50 mM KCl saturated with Ar, rotation rate 1500 RPM. B: 'Apparent' CER current j_{CER}', extracted from the average of the three ring scans in A. Also shown is a sigmoidal fit based on the generalized j-E curve including mass transfer effects (top panel). Middle panel shows the averaged forward and backward disk current from A, along with calculated partial CER and OER currents, assuming that $N_{Cl_2} \approx 0.12$. Bottom panel shows ε_{CER}, the corresponding molar selectivity towards CER. Current spikes were excluded from the calculation of both j_{CER}' and N_{Cl_2}.

quite effectively dislodged these bubbles, after which they scurried across the rotating electrode tip causing occasional current spikes (Fig. 3A, top and middle panel). Despite this, subsequent ring scans now show rather reproducible behaviour in the presence of the wire. Catastrophic collection failure, such as in Fig. 1, is avoided, even under intense gas-evolving conditions. In the potential region 1.46–1.53 V, where virtually all disk current is due to the CER, the collection factor has a value of about $N_{Cl_2} = 0.12$. This value is roughly 50% lower than the value of about 0.24 that we normally measured for chlorine collection under these conditions [42,43]. Considering that the value of 0.12 is reached in the forward scan of the first cycle, where the tip is completely free of bubbles, we may conclude that the wire causes this deviation in N_{Cl_2}. It also implies that N_{Cl_2} stays quite constant as a function of time, because approximately the same value is reached irrespective of the cycle number or scan direction. After 1.55 V, N_{Cl_2} apparently decreases due to an increasing OER contribution to the current on the disk.

The absolute values of the ring current densities from the three scans were averaged and smoothed, and termed 'apparent CER current', $j_{CER}{}'$. They are shown in the top panel of Fig. 3B. In this calculation, potential regions containing current spikes, such as near 1.65 V in scan 2, were excluded (see Fig. S1 for details). The resulting data is reminiscent of a typical sigmoid-shaped j-E curve, where initially the current is activation controlled and rises exponentially, but then crosses over into a constant diffusion limited value. To investigate the ring behaviour, $j_{CER}{}'$ was fitted using the 'anodic branch':

$$j = j_0 \left(\frac{e^{\alpha f \eta}}{1 + \frac{j_0}{j_L^{an}} e^{\alpha f \eta}} \right) \tag{2}$$

In Eq. (2), j_L^{an} is the anodic diffusion-limiting current, and $f = {}^{F}/_{(RT)}$. The model fits $j_{CER}{}'$ rather well (Fig. 3B, top), suggesting that the ring current, despite the intensive evolution of gas on the tip and presence of the wire, is quite well-behaved. The used value of α was 1.1, which slightly underestimated the exponential rise at the foot of the wave, but gave the best fit in the diffusion limited region. This allowed us to calculate a value of 6.74 mA $cm^{-2}{}_{Disk}$ for j_L^{an} measured on the ring. Furthermore, the CER diffusion-limitation on the disk that would be expected on the basis of the Levich equation is 61.16 mA $cm^{-2}{}_{Disk}$. From these values, the ring chlorine collection factor becomes $N_{Cl_2} = \frac{6.74}{61.16} \approx 0.11$ near 1.65 V. This value matches well with that measured in regimes of low current density (0.12), and implies that the Ti wire keeps N_{Cl_2} constant, irrespective of high or low gas evolution intensities. Taking $N_{Cl_2} = 0.12$, and under the reasonable assumption that no other processes besides the OER and CER are occurring on the disk, we then calculated j_{CER} and j_{OER}, the partial CER and OER current densities, by using

$$j_{OER} = j_D - j_{CER} = j_D - \left({}^{j_{CER}{}'}/_{N_{Cl_2}} \right) \tag{3}$$

where j_D are the averaged forward and backward disk current densities of the three scans. The results (Fig. 3B, middle) suggest that whereas CER becomes diffusion limited, OER activity rises continuously, as transport phenomena play a much smaller role for this reaction. This is reflected in the molar selectivity towards CER (bottom), which decreases sharply with increasing potential. From these results, one can assume that OER always becomes the dominant reaction if the potential is high enough, regardless of the chloride concentration, which has important implications for the selectivity between the two.

In experiments with an even further extended scan window, we noticed an apparent decrease of CER rates at potentials above 1.65 V vs. RHE (see Figs. S1 and S3). At the high potential limit, it is likely that the formation hypochlorous acid starts competing with CER. Hypochlorous acid cannot be detected by the ring under these conditions [43]. The occurrence of this reaction has been hypothesized and evidenced previously [46–49], though indirectly and via off-line methods. We believe this is the most direct result thus-far that suggests the CER crosses over into hypochlorous acid evolution at very high overpotentials. An appreciable decrease in disk activity is also apparent during these experiments, which is most likely due to mechanical shear from intense oxygen evolution and oxidative degradation of the GC support [50]. These observations demonstrate that the possibility of extending RRDE methods into wider potential windows could lead to interesting new insights. The wire affects N quite differently depending on whether gaseous Cl_2 or dissolved $[Fe(CN)_6]^{-4}$ is collected (see Fig. S4). The value for Cl_2 collection in 1 M HCl was $N_{Cl_2} \approx 0.13$, similar to results in Fig. 3, though it dropped to slightly lower values during very vigorous gas evolution ($j_D > 0.5$ A cm^{-2}). Subsequent measurements in 0.1 M KOH + 1 M KCl + 10 mM $K_3[Fe(CN)_6]$, while ensuring that the wire stayed in the exact same position, yielded $N = 0.197$ for $[Fe(CN)_6]^{-4}$. The latter value increased to 0.212 when the wire was moved slightly further away, and became 0.252 when the wire was completely removed, which is close to the ideal theoretical value of 0.258. During the ferri/ferrocyanide experiments, the wire likely lowers N by distorting the fluid dynamics near the surface; during gas evolution, this effect is compounded by gas bubbles that are forced off the electrode surface near the point of the wire. These gas bubbles probably increase the flow distortion, and are themselves not quantified by the ring, both of which lead to a lowering of the collection efficiency. One can expect that the actual value of N when placing a wire is not universal, but depends on factors such as the wire length and thickness, and the geometry of the electrode tip.

In conclusion, it can be stated that the mounted wire aids in bubble removal, which keeps N_{Cl_2} more constant and prevents ring collection failure during vigorous gas evolution, but it also causes the value of N_{Cl_2} to deviate strongly from theoretical values, meaning that an empirical correction would be needed. There are also practical disadvantages to the wire approach; the mounting of the wire and keeping it at the required position proved to be quite precarious. An incorrectly placed wire may easily scratch and damage the tip surface.

3.3. RRDE voltammetry experiments and the effect of a poly-dopamine coating

The observation in Section 3.2 that macroscopic gas bubbles universally appear at the disk-Teflon boundary, suggests that gas bubbles that form on the disk surface 'become stuck' on the Teflon surface as they are swept outward. However, it is likely that bubbles nucleate not so much on the hydrophilic electrode itself, but on the Teflon spacer in-between the disk and the ring [23], caused by a sudden gas concentration increase in the solution that flows past the spacer [51]. The problem of bubble nucleation may be aggravated when using rotating electrode tips with interchangeable disk electrodes. While offering significant experimental flexibility, the surface of such tips will always have at least micrometer-sized imperfections at the boundaries between the disk, spacer and ring, irregularities which favour bubble nucleation and growth.

A promising method of disfavouring bubble nucleation would be to decrease the hydrophobicity of the electrode tip material. We attempted this by coating the pre-assembled electrode tip with polydopamine (p-DA), a hydrophilic polymer that preferentially deposits on hydrophobic, organic surfaces [52,53]. Successful p-DA deposition on both the Teflon spacer and PEEK outer shroud was evidenced by a large increase of tip wettability after treatment. Alternatively, we also tried coating the ejected Teflon spacers with a water insoluble but

hydrophilic polymer, such as poly(4-vinylpyridine). However, an even coating could not easily be achieved, and the layer was easily damaged upon reinsertion of the spacer into the RRDE tip, which requires pressing.

After the p-DA deposition procedure, some degree of DA or p-DA adsorption on the Pt surfaces was suggested by a large drop in the open-circuit potential, which was monitored during the coating (Fig. S5). However, after the coating treatment we were able to recover the Pt surface readily via electropolishing (Fig. S6), suggesting that this adsorption is minor and not problematic. We then measured the effect of the coating on the collection of O_2 and H_2. Two different gases were tested, since electrochemical bubble nucleation and growth behaviour can depend heavily on the type of gas evolved [56–58]; it was therefore of interest to see whether the coating would have the same effect on each gas.

Cyclic voltammograms in Fig. 4A show hydrogen collection experiments on a Pt-Pt RRDE, at 10 mV s^{-1}. In absence of the p-DA coating, the electrode initially has a collection efficiency that approaches 0.251, which is very close to the ideal theoretical value of 0.258. At potentials lower than −18 mV, the value of N_{H_2} drops sharply and does not recover for the remainder of the scan, similar to the results of Fig. 1. Around this potential, the HER disk current density is −2 mA cm^{-2}, a value quite similar to that found by Frazer et al. for ring failure for HER collection in a i_R vs. i_D plot at approximately −1.5 mA cm^{-2}, under 1200 RPM [54]. The effect of the p-DA coating is a mild but consistent increase in N_{H_2} during the negative scan. Unfortunately, the coating does not influence the potential where the ring collection starts to fail, nor is it able to help recovery of the ring as the potential is swept back to where the electrode is less active. During amperometry experiments in Fig. 4B and C, where H_2 is continuously generated and collected at gradually increasing current density steps, the main effect of the p-DA coating is again a small but visible increase in N_{H_2}, its value increasing from 0.249 to 0.256 in presence of the coating. In Fig. 4B, the value stays quite constant up until 195 s, irrespective of the coating, but N_{H_2} drops dramatically as the disk current is increased to −4.6 mA cm^{-2}. The failure of N_{H_2} is evident here from a dramatic decrease in both the ring current density and disk current density. After the potential step at 240 s, the experiment is completely dominated by the erratic effects of bubbles accumulating on the tip. Fig. 4C shows a series of shorter amperometry steps, with smaller current increases that are specifically targeted at the region of 140–195 s in Fig. 4B, where collection failure starts to appear on the uncoated tip. One can observe that the p-DA coating helps maintain N_{H_2} for a longer time in this experiment. Comparing the disk currents where N_{H_2} starts to deviate, it can be said that the p-DA enables reliable collection measurements under currents that are roughly 50% higher than the uncoated tip.

In Fig. 5, we explored the collection factor for OER on Pt, as well as the effect of a p-DA coating, using a similar procedure as in the H_2 experiments. Pt was used for O_2 generation instead of IrO_x, since we wanted to compare the collection behaviour of 'pure OER' on a non-porous catalyst, free from possible extra collection complications caused by gas bubbles in pores (see also Section 1). It must be noted that Pt experiences a strong growth of multilayer oxides under OER potentials; a significant fraction of disk current (as much as 20–30% [55]) can be consumed in the formation of the oxide layer parallel to OER, meaning that the OER faradaic efficiency (and concomitantly the expected value for N_{O_2}) is usually lower than 100%. As such, we will primarily discuss results from relative collection efficiencies, under the assumption that the OER faradaic efficiency has the same value for each experiment. To minimize the variational effect of PtO_x formation on the OER faradaic efficiency, a moderately thick oxide layer was grown prior to each experiment. The OER cyclic sweep was started at 1.30 V, well before the onset of OER on Pt, and in the amperometry, a pre-step of 1.45 V vs. RHE was applied for 15 s.

In the forward sweep in Fig. 5A, the ring current density increases significantly when a p-DA coating is applied. N_{O_2} correspondingly changes from 0.14 to 0.20 in the initial stages of the forward scan, which is a much larger collection increase (roughly 40%) compared to the H_2 collection experiments in Fig. 4A, where N_{H_2} is initially close to the ideal value. The transport of O_2 gas from the disk to the ring is thus somehow impaired in comparison with that of H_2. This is likely caused by the same underlying principles that lead to divergent behaviour in electrochemical growth of O_2 and H_2 bubbles, as previously reported [56–58]. The low O_2 collection efficiency is considerably

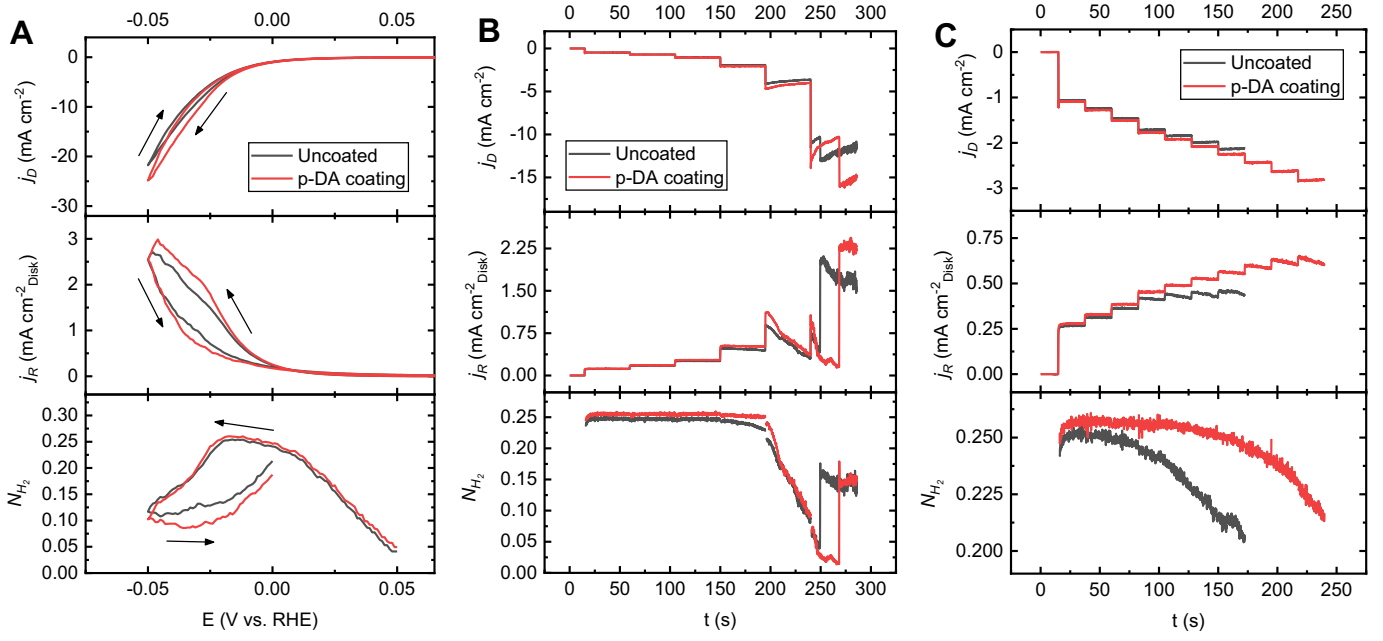

Fig. 4. H_2 collection experiments on a Pt-Pt RRDE tip, and the effect of a p-DA coating on the collection efficiency. Displayed across the graphs are disk (top panels) and ring current densities (middle panels), bottom panels show the collection factor N_{H_2}. A: Cyclic voltammograms, scan rate 10 mV s^{-1}. Arrows indicate scan direction. B: Amperometry using 45 s steps at stepwise more negative potentials, chosen to gradually increase HER rates. C: Amperometry using 22.5 s steps and smaller potential steps, resulting currents targeted around the region where N_{H_2} starts to fail in B. The Pt ring was fixed at 0.4 V to detect H_2. Solution: 0.1 M $HClO_4$ saturated with Ar, rotation rate 1500 RPM. The first 0.5 s of each amperometry step is not shown for N, because of charging effects distorting its value.

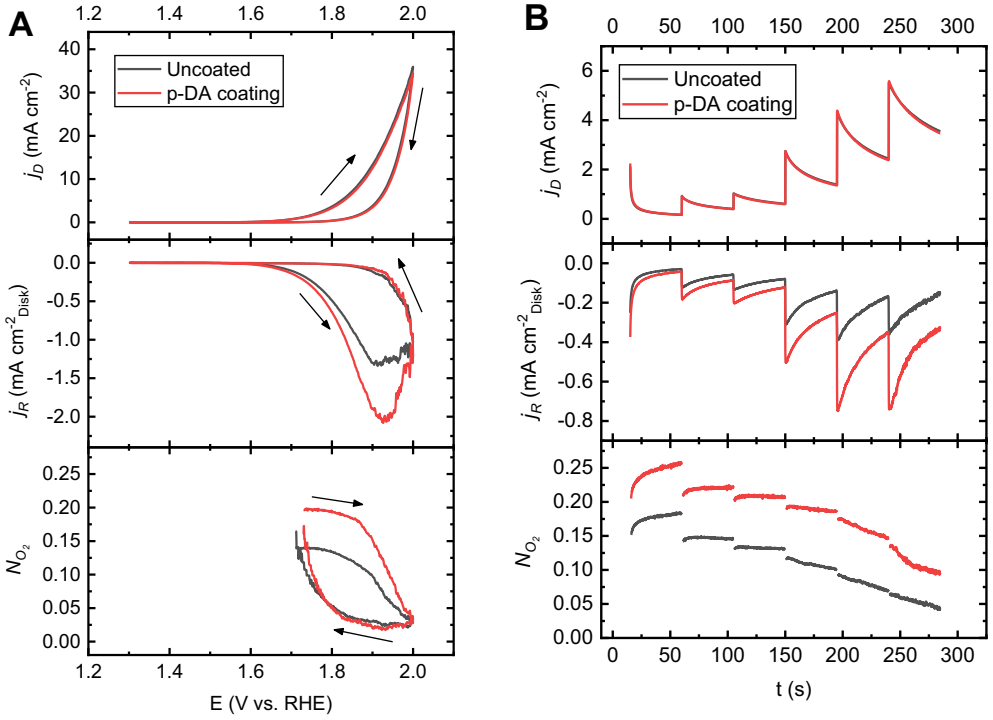

Fig. 5. O_2 collection experiments on a Pt-Pt RRDE tip, and the effect of a p-DA coating on the collection efficiency. Displayed across the graphs are disk (top panels) and ring current densities (middle panels), bottom panels show the collection factor N_{O_2}. A: Cyclic voltammograms, scan rate 10 mV s^{-1}. B: Amperometry using 45 s steps at stepwise larger positive potentials, chosen to gradually increase OER rates. The Pt ring was fixed at 0.4 V to detect O_2. Solution: 0.1 M $HClO_4$ saturated with Ar, rotation rate 1500 RPM. The first 0.5 s of each amperometry step is not shown for *N*, because of charging effects distorting its value.

improved by the p-DA coating. On the other hand, N_{O_2} fails irreversibly once the disk current density increases past a certain threshold, regardless of the coating, similar to the H_2 experiments. Amperometry experiments involving stepwise increases in disk current density (Fig. 5B) show that N_{O_2} again has significantly higher values at all times. However, in both cases it starts decreasing significantly after 145 s, meaning that the current density where transport to the ring starts to be negatively affected is virtually unchanged. Summing up the findings from the effect of a p-DA coating on the RRDE tip: it has a favourable effect on the collection efficiency of both H_2 and O_2; but the improvement of O_2 collection appears more significant, and the mechanism of improvement seems inherently different between the two gases. For H_2 collection, the current density threshold for irreversible collection failure is only mildly improved; in case of O_2, the collection behaviour before the onset of ring failure is greatly improved.

Evidently, while the p-DA coating has a favourable effect on the general collection behaviour of the tip, and allows a mild extension of disk current densities that can reliably be measured, irreversible ring failure still sets in rapidly once a certain threshold activity is exceeded. It may certainly be possible to further improve the RRDE collection behaviour using the avenue of tip coating. The p-DA coating procedure could be further optimized [59]; It should also be possible to utilize coating layers that are even more hydrophilic than p-DA, to further lower the nucleation probability of gas bubbles during measurement.

4. Conclusions

In this work, we investigated the vulnerability of disk-to-ring transport during gas-collection experiments on a rotating ring-disk electrode, as well as two methods for improving this gas collection behaviour. Use of a thin wire to selectively dislodge bubbles at the disk-spacer boundary prevented ring failure due to gas bubbles, and made the collection factor more reproducible as a function of time. The wire allowed chlorine collection experiments under intense gas-evolving conditions, although it caused the measured values to become lower than theoretical predictions, and was challenging to implement in practice. If many wire experiments are desired, it is recommended to construct a dedicated mechanical setup coupled to a micrometer system, to aid in properly mounting the wire and keeping it in position. Application of a hydrophilic poly-dopamine coating on the electrode tip led to moderate improvements in the collection of oxygen and hydrogen. Whereas for hydrogen collection, the current density threshold before ring failure was increased by roughly 50%, for oxygen instead the overall collection efficiency increased.

Acknowledgements

This research received funding from the Netherlands Organization for Scientific Research (NWO) in the framework of the fund New Chemical Innovations, project 731.015.204 ELECTROGAS, with financial support of Akzo Nobel Chemicals, Shell Global Solutions, Magneto Special Anodes (an Evoqua Brand) and Elson Technologies.

We also wish to thank professor Henry S. White for very meaningful discussions about a wide range of gas bubble-related topics.

Appendix A. Supplementary data

Supplementary data to this article can be found online at https://doi.org/10.1016/j.jelechem.2019.113363.

References

[1] A.J. Bard, L.R. Faulkner, et al., Fundamentals and applications, Electrochem. Methods 2 (2001) 482.
[2] H. Liu, C. Song, L. Zhang, J. Zhang, H. Wang, D.P. Wilkinson, A review of anode catalysis in the direct methanol fuel cell, J. Power Sources 155 (2) (2006) 95–110.
[3] I.V. Kadija, V.M. Nakić, Ring electrode on rotating disc as a tool for investigations of gas-evolving electrochemical reactions, J. Electroanal. Chem. Interfacial Electrochem. 34 (1) (1972) 15–19.

[4] S. Hessami, C.W. Tobias, In-situ measurement of interfacial PH using a rotating ring-disk electrode, AICHE J. 39 (1) (1993) 149–162.
[5] Y. Qiu, L. Xin, W. Li, Electrocatalytic oxygen evolution over supported small amorphous Ni–Fe nanoparticles in alkaline electrolyte, Langmuir 30 (26) (2014) 7893–7901.
[6] J. Scholz, M. Risch, K.A. Stoerzinger, G. Wartner, Y. Shao-Horn, C. Jooss, Rotating ring–disk electrode study of oxygen evolution at a perovskite surface: correlating activity to manganese concentration, J. Phys. Chem. C 120 (49) (2016) 27746–27756.
[7] Q. Gao, C. Ranjan, Z. Pavlovic, R. Blume, R. Schlögl, Enhancement of stability and activity of MnOx/Au electrocatalysts for oxygen evolution through adequate electrolyte composition, ACS Catal. 5 (12) (2015) 7265–7275.
[8] P. Westbroek, E. Temmerman, In line measurement of chemical oxygen demand by means of multipulse amperometry at a rotating Pt ring — Pt/PbO2 disc electrode, Anal. Chim. Acta 437 (1) (2001) 95–105.
[9] N.D. Popović, D.C. Johnson, A ring–disk study of the competition between anodic oxygen-transfer and dioxygen-evolution reactions, Anal. Chem. 70 (3) (1998) 468–472.
[10] J. Kim, X. Yin, K.-C. Tsao, S. Fang, H. Yang, Ca2Mn2O5 as oxygen-deficient perovskite electrocatalyst for oxygen evolution reaction, J. Am. Chem. Soc. 136 (42) (2014) 14646–14649.
[11] Y. Lee, J. Suntivich, K.J. May, E.E. Perry, Y. Shao-Horn, Synthesis and activities of rutile IrO2 and RuO2 nanoparticles for oxygen evolution in acid and alkaline solutions, J. Phys. Chem. Lett. (pH 1) (2012) 399–404.
[12] X. Yu, M. Zhang, W. Yuan, G. Shi, A high-performance three-dimensional Ni–Fe layered double hydroxide/graphene electrode for water oxidation, J. Mater. Chem. A 3 (13) (2015) 6921–6928.
[13] D. Chen, C.-L. Dong, Y. Zou, D. Su, Y.-C. Huang, L. Tao, S. Dou, S. Shen, S. Wang, In situ evolution of highly dispersed amorphous CoOx clusters for oxygen evolution reaction, Nanoscale 9 (33) (2017) 11969–11975.
[14] A.T. Swesi, J. Masud, M. Nath, Nickel selenide as a high-efficiency catalyst for oxygen evolution reaction, Energy Environ. Sci. 9 (5) (2016) 1771–1782.
[15] P. Steegstra, E. Ahlberg, In situ PH measurements with hydrous iridium oxide in a rotating ring disc configuration, J. Electroanal. Chem. 685 (2012) 1–7.
[16] R.E.F. Einerhand, W.H.M. Visscher, E. Barendrecht, Hydrogen production during zinc deposition from alkaline zincate solutions, J. Appl. Electrochem. 18 (6) (1988) 799–806.
[17] J. Horkans, Determination of partial currents for CuNi and CuCo electrodeposition using rotating ring-disk electrodes, J. Electrochem. Soc. 138 (2) (1991) 411.
[18] C.C.L. McCrory, S. Jung, J.C. Peters, T.F. Jaramillo, Benchmarking heterogeneous electrocatalysts for the oxygen evolution reaction, J. Am. Chem. Soc. 135 (45) (2013) 16977–16987.
[19] J. Suntivich, K.J. May, H.A. Gasteiger, J.B. Goodenough, Y. Shao-Horn, A perovskite oxide optimized for oxygen evolution catalysis from molecular orbital principles, Science (80-.) 334 (6061) (2011) 1383–1385.
[20] S. Zhao, Y. Wang, J. Dong, C.-T. He, H. Yin, P. An, K. Zhao, X. Zhang, C. Gao, L. Zhang, et al., Ultrathin metal–organic framework nanosheets for electrocatalytic oxygen evolution, Nat. Energy 1 (November) (2016) 16184.
[21] J. Scholz, M. Risch, G. Wartner, C. Luderer, V. Roddatis, C. Jooss, Tailoring the oxygen evolution activity and stability using defect chemistry, Catalysts 7 (5) (2017) 139.
[22] Y. Hu, Y.V. Tolmachev, D.A. Scherson, Rotating ring-disk studies of oxidized nickel hydrous oxide: oxygen evolution and pseudocapacitance, J. Electroanal. Chem. 468 (1) (1999) 64–69.
[23] I.V. Kadija, B.Ž. Nikolić, A.R. Despić, Mass transfer during gas evolution on the rotating double-ring electrode, J. Electroanal. Chem. Interfacial Electrochem. 57 (1) (1974) 35–52.
[24] S.R. German, M.A. Edwards, Q. Chen, Y. Liu, L. Luo, H.S. White, Electrochemistry of single nanobubbles. Estimating the critical size of bubble-forming nuclei for gas-evolving electrode reactions, Faraday Discuss. 193 (2016) 223–240.
[25] H. Ren, S.R. German, M.A. Edwards, Q. Chen, H.S. White, Electrochemical generation of individual O2 nanobubbles via H2O2 oxidation, J. Phys. Chem. Lett. 8 (11) (2017) 2450–2454.
[26] N.M. Marković, T.J. Schmidt, V. Stamenković, P.N. Ross, Oxygen reduction reaction on Pt and Pt bimetallic surfaces: a selective review, Fuel Cells 1 (2) (2001) 105–116.
[27] K. Ben Liew, W.R.W. Daud, M. Ghasemi, J.X. Leong, S. Su Lim, M. Ismail, Non-Pt catalyst as oxygen reduction reaction in microbial fuel cells: a review, Int. J. Hydrog. Energy 39 (10) (2014) 4870–4883.
[28] D. Geng, Y. Chen, Y. Chen, Y. Li, R. Li, X. Sun, S. Ye, S. Knights, High oxygen-reduction activity and durability of nitrogen-doped graphene, Energy Environ. Sci. 4 (3) (2011) 760.
[29] H. Vogt, R.J. Balzer, The bubble coverage of gas-evolving electrodes in stagnant electrolytes, Electrochim. Acta 50 (10) (2005) 2073–2079.
[30] H. Vogt, The actual current density of gas-evolving electrodes—notes on the bubble coverage, Electrochim. Acta 78 (2012) 183–187.
[31] I.S. Filimonenkov, S.Y. Istomin, E.V. Antipov, G.A. Tsirlina, E.R. Savinova, Rotating ring-disk electrode as a quantitative tool for the investigation of the oxygen evolution reaction, Electrochim. Acta 286 (2018) 304–312.
[32] A.R. Zeradjanin, Frequent pitfalls in the characterization of electrodes designed for electrochemical energy conversion and storage, ChemSusChem 11 (8) (2018) 1278–1284.
[33] H.K. Kuiken, E.P.A.M. Bakkers, H. Ligthart, J.J. Kelly, The rotating ring-ring electrode. Theory and experiment, J. Electrochem. Soc. 147 (3) (2000) 1110.
[34] X. Zhu, K. Gupta, M. Bersani, J.A. Darr, P.R. Shearing, D.J.L. Brett, Electrochemical reduction of carbon dioxide on copper-based nanocatalysts using the rotating ring-disc electrode, Electrochim. Acta 283 (2018) 1037–1044.
[35] L. Bai, B.E. Conway, Electrochemistry of anodic F2 evolution at carbon electrodes: bubble adherence effects in the kinetics at rotating cone electrodes, J. Appl. Electrochem. 18 (6) (1988) 839–848.
[36] E. Kirowa-Eisner, E. Gileadi, The rotating cone electrode, J. Electrochem. Soc. 123 (1) (1976) 22.
[37] L.J.J. Janssen, Mass transfer at rotating ring-cone electrodes, J. Appl. Electrochem. 22 (11) (1992) 1091–1094.
[38] B. Miller, Rotating ring-disk study of the silver electrode in alkaline solution, J. Electrochem. Soc. 117 (4) (1970) 491.
[39] T. Nakagawa, C.A. Beasley, R.W. Murray, Efficient electro-oxidation of water near its reversible potential by a mesoporous IrOx nanoparticle film, J. Phys. Chem. C 113 (30) (2009) 12958–12961.
[40] Y. Zhao, N.M. Vargas-Barbosa, E.A. Hernandez-Pagan, T.E. Mallouk, Anodic deposition of colloidal iridium oxide thin films from hexahydroxyiridate(IV) solutions, Small 7 (14) (2011) 2087–2093.
[41] Y. Zhao, E.a. Hernandez-Pagan, N.M. Vargas-Barbosa, J.L. Dysart, T.E. Mallouk, A high yield synthesis of ligand-free iridium oxide nanoparticles with high electrocatalytic activity, J. Phys. Chem. Lett. 2 (5) (2011) 402–406.
[42] J.G. Vos, T.A. Wezendonk, A.W. Jeremiasse, M.T.M. Koper, MnOx/IrOx as selective oxygen evolution electrocatalyst in acidic chloride solution, J. Am. Chem. Soc. 140 (32) (2018) 10270–10281.
[43] J.G. Vos, M.T.M. Koper, Measurement of competition between oxygen evolution and chlorine evolution using rotating ring-disk electrode voltammetry, J. Electroanal. Chem. 819 (October) (2018) 260–268.
[44] M. Alkan, M. Oktay, M.M. Kocakerim, M. Çopur, Solubility of chlorine in aqueous hydrochloric acid solutions, J. Hazard. Mater. 119 (1–3) (2005) 13–18.
[45] R.K.B. Karlsson, A. Cornell, Selectivity between oxygen and chlorine evolution in the chlor-alkali and chlorate processes, Chem. Rev. 116 (5) (2016) 2982–3028.
[46] F. Dionigi, T. Reier, Z. Pawolek, M. Gliech, P. Strasser, Design criteria, operating conditions, and nickel-iron hydroxide catalyst materials for selective seawater electrolysis, ChemSusChem 9 (9) (2016) 962–972.
[47] J. Juodkazytė, B. Šebeka, I. Savickaja, M. Petrulevičienė, S. Butkutė, V. Jasulaitienė, A. Selskis, R. Ramanauskas, Electrolytic splitting of saline water: durable nickel oxide anode for selective oxygen evolution, Int. J. Hydrog. Energy 44 (12) (2019) 5929–5939.
[48] S. Dresp, F. Dionigi, S. Loos, J. Ferreira de Araújo, C. Spöri, M. Gliech, H. Dau, P. Strasser, Direct electrolytic splitting of seawater: activity, selectivity, degradation, and recovery studied from the molecular catalyst structure to the electrolyzer cell level, Adv. Energy Mater. 8 (22) (2018), 1800338.
[49] I. Sohrabnejad-Eskan, A. Goryachev, K.S. Exner, L.A. Kibler, E.J.M. Hensen, J.P. Hofmann, H. Over, Temperature-dependent kinetic studies of the chlorine evolution reaction over RuO2 (110) model electrodes, ACS Catal. 7 (4) (2017) 2403–2411.
[50] S. Geiger, O. Kasian, A.M. Mingers, S.S. Nicley, K. Haenen, K.J.J. Mayrhofer, S. Cherevko, Catalyst stability benchmarking for the oxygen evolution reaction: the importance of backing electrode material and dissolution in accelerated aging studies, ChemSusChem 10 (21) (2017) 4140–4143.
[51] S.F. Jones, G.M. Evans, K.P. Galvin, Bubble nucleation from gas cavities — a review, Adv. Colloid Interf. Sci. 80 (1) (1999) 27–50.
[52] Z.-Y. Xi, Y.-Y. Xu, L.-P. Zhu, Y. Wang, B.-K. Zhu, A facile method of surface modification for hydrophobic polymer membranes based on the adhesive behavior of poly (DOPA) and poly(dopamine), J. Membr. Sci. 327 (1–2) (2009) 244–253.
[53] J. Jiang, L. Zhu, L. Zhu, B. Zhu, Y. Xu, Surface characteristics of a self-polymerized dopamine coating deposited on hydrophobic polymer films, Langmuir 27 (23) (2011) 14180–14187.
[54] E.J. Frazer, I.C. Hamilton, The estimation of the coulombic efficiency of zinc electrodeposition by measurement of current efficiencies at a rotating ring disc electrode, J. Appl. Electrochem. 16 (3) (1986) 387–392.
[55] V.I. Birss, A study of the transition from oxide growth to O[Sub 2] evolution at Pt electrodes in acid solutions, J. Electrochem. Soc. 130 (8) (1983) 1688.
[56] L.J.J. Janssen, C.W.M.P. Sillen, E. Barendrecht, S.J.D. van Stralen, Bubble behaviour during oxygen and hydrogen evolution at transparent electrodes in KOH solution, Electrochim. Acta 29 (5) (1984) 633–642.
[57] S.G. da Cruz, A.J.B. Dutra, M.B.M. Monte, The influence of some parameters on bubble average diameter in an electroflotation cell by laser diffraction method, J. Environ. Chem. Eng. 4 (3) (2016) 3681–3687.
[58] H. Matsushima, T. Nishida, Y. Konishi, Y. Fukunaka, Y. Ito, K. Kuribayashi, Water electrolysis under microgravity, Electrochim. Acta 48 (28) (2003) 4119–4125.
[59] R.A. Zangmeister, T.A. Morris, M.J. Tarlov, Characterization of polydopamine thin films deposited at short times by autoxidation of dopamine, Langmuir 29 (27) (2013) 8619–8628.